Contribution of Gas and Electric Stoves to Residential Ultrafine Particle Concentrations between 2 and 64 nm: Size Distributions and Emission and Coagulation Rates

LANCE WALLACE,* FANG WANG, CYNTHIA HOWARD-REED, AND ANDREW PERSILY

National Institute of Standards and Technology, 100 Bureau Drive, MS8633, Gaithersburg, Maryland 20899

Received May 27, 2008. Revised manuscript received September 12, 2008. Accepted September 18, 2008.

Three indoor sources (a gas stove, an electric stove, and an electric toaster oven) of ultrafine particles (UFPs) have been studied in an instrumented test house on the campus of the National Institute of Standards and Technology (NIST). Previous studies have reported the concentration of ultrafine particles indoors due to cooking, but have been limited to particles with diameters greater than 10 nm. New technology now makes it possible to measure particles as small as 2 nm. Therefore, NIST conducted a study to measure typical concentrations and estimate emission rates and coagulation rates of UFPs in the size range from 2 to 64 nm. More than 150 tests were completed. Peak concentrations from the gas and electric stovetop burners/coils occurred at a particle size of approximately 5 nm. Total number concentrations were as much as 10 times greater than reported in previous studies of particle sizes above 10 nm. Because of these high concentrations of very small particles, coagulation was the dominant process affecting the evolution of the size distribution after the source was turned off. The observed number concentration changes due to coagulation were fit by models including corrections for van der Waals and viscosity forces and fractal shapes. Indoor/outdoor ratios indicated that less than 5% of the <10 nm particles penetrated the house. This suggests that outdoor sources of these ultrafine particles will not contribute substantially to human exposure if indoor sources are present.

Introduction

Ultrafine particles (UFPs), particles with an aerodynamic diameter of <100 nm, have been shown to have toxic effects on mice, rats, and human cells (*1*). Human health effects such as oxidative stress and even mortality are also suspected (*2*−*4*).

Major outdoor sources of UFP include auto exhaust as well as atmospheric chemical reactions (*5, 6*). The major indoor source is cooking (*7*−*9*); tobacco smoke appears not to have a strong ultrafine component (*10*). A number of other indoor sources have also been identified (*11, 12*), but most of these are used less widely and less frequently than cooking appliances.

Most of these indoor studies have employed measurement devices that cannot measure below 10 nm. However, there have been indications that sources may produce considerable particle numbers below 10 nm. For example, gas stovetop burners used to boil water appeared to have peaks at or possibly below 10 nm (*13*). Recently, a nano differential mobility analyzer (nano-DMA) capable of extending our knowledge to the sub 10 nm region was developed (*14*).

About 40% of U.S. residences have gas stoves, 60% have electric stoves, and 56% have electric toaster ovens, so these were selected as the sources of interest (*15*).

The fundamental objective of this study was to determine the effect of these kitchen appliances on indoor UFP concentrations, with particular attention to the sub 10 nm fraction. The approach was to measure concentrations in a well-characterized uninhabited test house. Since the data are more useful if they can be applied to buildings of any size, estimates of size-resolved emission and coagulation rates were also developed.

Methods

This study employed a scanning mobility particle sizer (SMPS) (model 3936, TSI, Shoreview, MN), consisting of an electrostatic classifier (model 3080), a nano-DMA (model 3085), and a water-based condensation particle counter (CPC; model 3786). The classifier with the nano-DMA is considered a reference instrument for determining particle size, with an estimated uncertainty at the 60 and 100 nm diameters of 1% (*16*). The CPC has a stated uncertainty of 12% in the manufacturer specifications (*17*).

A bypass pump (model 3032, TSI) with a critical flow orifice (model W-13-SS, O'Keefe, Trumbull, CT) was added to the system to increase the aerosol particle flow rate from 0.01 to 0.025 L/s. This addition extended the range of detectable particles down to approximately 2 nm in diameter in the most favorable case of water-soluble particles (*18*).

The sheath flow was set at 0.25 L/s to maintain a 10/1 sheath/aerosol flow ratio. Internal losses due to diffusion were reduced as much as possible by using no external tubing and removing the impactor. These changes reduced diffusion losses from 99.9% for the smallest particles (2.02 nm) to 98.4%, a better than 10-fold improvement. The remaining diffusion losses are due to the internal geometry of the SMPS (penetration through the bipolar neutralizer, classifier, and CPC; losses in the tubing connecting the nano-DMA and the CPC) and cannot be reduced further. These diffusion losses have been calculated and verified experimentally by the manufacturer (*19*) and are supplied as supplemental corrections in the manufacturer's software. However, uncertainties in these corrections were not reported.

The scan rate was set at 2.5 min (2 min of measurement, 30 s for the voltage to return to the baseline), covering 97 size categories from 2 to 64 nm.

The National Institute of Standards and Technology (NIST) test house is a manufactured house with a volume of 340 m^3 (floor area 140 m^2, average height 2.4 m; see the floor plan in the Supporting Information, Figure S1). A central forced-air fan was kept on during most of the tests to improve mixing. Air change rates are calculated using a dedicated gas chromatograph with an electron capture detector (GC/ECD)

* Corresponding author address: 11568 Woodhollow Ct., Reston, VA 20191 (retired from the U.S. Environmental Protection Agency); phone: (703) 620-4543; fax: (571) 201-8953; e-mail: lwallace73@comcast.net.

10.1021/es801402v CCC: $40.75
Published on Web 10/30/2008

to measure the decay of a tracer gas (SF_6) that is injected periodically into the living room (*20*).

Sampling was conducted from before the beginning of the cooking period to variable times afterward, ranging from an hour to a day. For the majority of tests, the SMPS was in the master bedroom (MBR), chosen to represent house-wide concentrations. When the SMPS was in the master bedroom, it was approximately 12 m away from the cooking devices in the kitchen.

Indoor/outdoor number concentrations were measured sequentially on a 10 min cycle (four scans each) using an automatic switching mechanism developed by NIST technicians. These measurements were designed to provide estimates of the penetration of outdoor ultrafine particles into the house.

We studied a gas stove, electric stove, and electric toaster oven. To approximate exposures of the cook, the SMPS was placed in the kitchen for some tests. (In these cases, no estimate of emission rates was attempted, due to the inhomogeneity of the concentrations and the difficulty of determining the volume to be used in the calculation.) The UFP size distributions produced by the gas flame and gas oven alone (no pots or food) were characterized in 42 experiments. For these experiments, the stand for supporting pots and pans was removed, and only the diffuser splitting the gas flow into multiple jets was retained. The size distributions produced by boiling water and several types of cooking (frying, stir-frying, baking, making toast) were characterized in a second set of 36 experiments with the gas stove. The electric stove was employed for a set of 74 experiments with and without food or water. Finally, 18 experiments, 12 without food and 6 with food, were carried out on the electric toaster oven. Four of these experiments were carried out with the toaster oven and SMPS in the master bedroom with the door closed, an effort to imitate worst-case scenarios in a small room or apartment.

We measured the size distribution before, during, and after the appliances were operated. We estimated emission rates by dividing the maximum total number concentration observed near the beginning of the decay period by the cooking time (time the source was on) and multiplying by the house volume. This estimate ignores the losses due to air change, deposition, and coagulation. Since the source was often on for only a few minutes and the inverse of the air change and deposition rates is on the order of a few hours, the effect of these two loss terms is small. However, the coagulation effect is much larger, and therefore, the emission rates are all underestimates; more serious underestimates are obtained with longer source times.

The extension to <10 nm particles in this study has made it necessary to consider coagulation to a greater extent than previously. Coagulation is an increasingly important process as diameters decrease, due to increased Brownian motion and resulting increases in the collision rate. Coagulation dominates other loss processes such as air exchange and deposition for the particle sizes and number concentrations measured in this set of experiments. Coagulation theory as presented by Seinfeld and Pandis (*21*) was applied to calculate the second-to-second changes in the size distribution. An algorithm including the Fuchs correction for the transition and free molecular regimes was developed, validated by comparison with several known collision probabilities, and then applied to the observed evolution of size distributions during the decay phase. The algorithm is described in the Supporting Information.

The calculated collision probabilities need to be corrected for two additional forces: van der Waals interactions and viscosity effects. The van der Waals interaction occurs most strongly for the smallest particles; it consists of an attractive force brought about by the creation of dipoles in each particle as a result of random variations of the arrangement of internal charges in the particle and results in increasing the collision rate. The viscosity effect has the opposite result, but is often smaller than the van der Waals force in the free molecular and transition regimes. It occurs because of the resistance of the fluid to being "squeezed" out of the region between the two advancing particles.

The equations for the van der Waals and viscosity correction to the coagulation kernels are given by Jacobson and Seinfeld (*22*). These equations include a factor that depends on the composition of the particles: the Hamaker constant. Since we do not know the composition of the particles, we chose a value of 20 kT for the Hamaker constant, which is a common value for a number of different molecules (*23*). With this choice of the Hamaker constant, the van der Waals/viscosity "enhancement factor" varied from about 1 for particle pairs of >50 nm each to 2.7 for a pair of 2 nm particles. An alternative choice for the Hamaker constant is 200 kT, applicable to graphite and perhaps to some metals. Since our gas stove particles contain carbon, and the electric appliance particles may contain metals from the heating elements, the value of 200 kT may also be applicable, so we investigated its use. This choice leads to a larger range for the enhancement factor, up to 4.3.

Finally, yet another correction may be required if the particles agglomerate in such a way that their volumes obey a fractal power law: $V \sim L^x$, where L is a characteristic length and x is the fractal dimension. Fractal dimensions tend to range from 1.5 to 2.5 (*24*). Following Jacobson (*24*), we chose a fractal dimension of 1.7 to calculate a correction factor. However, electron micrographs suggest that the smallest combustion particles are spherical (*25*). Therefore, there may be a cutoff diameter below which the fractal correction is not required. On the basis of measurements near Los Angeles freeways, Jacobson and Seinfeld (*22*) suggest 24−27 nm as the cutoff.

The three correction factors (van der Waals/viscosity, fractal, and fractal with a cutoff), crossed with the two Hamaker constants of 20 and 200 kT, result in six different correction matrices that can be applied to the observed size-resolved number concentration decay curves.

For a given set of scans immediately following cutoff of the source, the kernels with the Fuchs correction were calculated, and then one of the six correction matrices was applied to determine the collision probabilities. Since the collision probabilities are given in terms of collisions per second, the number concentrations in each of the size categories must be updated each second and the calculations iterated 150 times to match the 2.5 min scan time of the SMPS. The change in number concentrations of the kth size category (ΔN_k) between successive scans due to coagulation alone was compared to the observed ΔN_k due to combined coagulation, air change, and deposition. To obtain an objective measure of the goodness of fit of the coagulation models, the number changes due to air change rates and deposition rates were estimated and subtracted from the observed ΔN_k. For the air change rates, we used the measured values at the time of each experiment; for the deposition rates, we used the results of Lai and Nazaroff (*26*). The goodness of fit was then estimated by selecting the model with the smallest sum of absolute differences between the calculated and predicted ΔN_k due to coagulation.

Results and Discussion

Concentrations, Size Distributions, and Emission Rates. Since most of the ultrafine particles are produced by the flame or the heating element, rather than the pots, pans, or food, the appliances were first investigated for their production of particles without any food or water being heated.

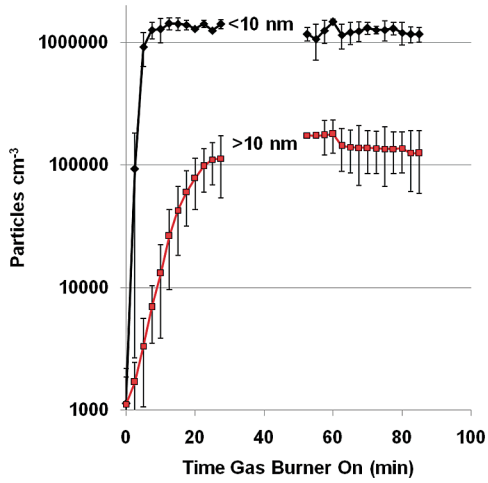

FIGURE 1. Growth to steady-state particle number concentrations from a single gas burner set on high (naked flame, no ringstand, no pot). Shown are the concentrations in the kitchen during the first and third half-hours of operation. (The SMPS was moved to the bedroom during the second and fourth half-hours.) Error bars are standard errors ($N = 3$).

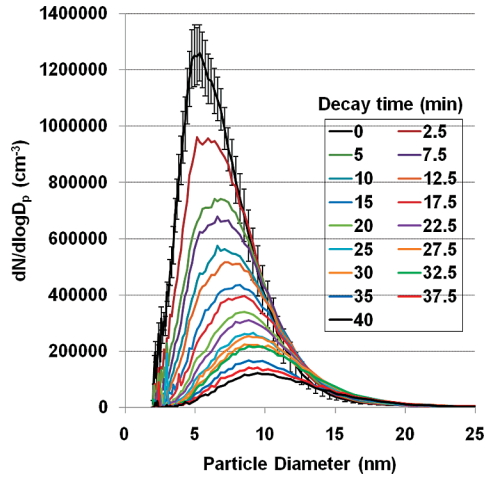

FIGURE 2. Evolution of the average size distribution from 11 gas burner experiments (burner on highest setting for 10 min (naked flame, no ringstand, no pot), SMPS in MBR). Error bars (standard errors) are shown for the maximum concentration reached immediately after the burner was turned off.

Gas Stove. The UFP size distributions produced by the gas flame and gas oven alone are provided in Table S1, Supporting Information. Three long-term (2 h) tests were carried out with a single burner operating to investigate growth toward steady-state particle concentrations. With the burner on high and the SMPS in the kitchen, the <10 nm particles reached asymptotic number concentrations of about 10^6 cm^{-3}, about 10 times the level of the >10 nm particles (Figure 1). The total gas flow for these experiments ranged between 489 and 501 L.

In 11 experiments, a single burner was activated in the "high" mode for varying times from 10 to 25 min. The gas flow rate for these and other single-burner experiments was 4.2 (SD = 0.3, $N = 28$) L/min. For the gas burner with no ringstand, the average initial size distribution (first scan after the burner was turned off) peaked at about 5.3 nm. The particle size mode then increased from 5 to nearly 10 nm over the next 40 min of the decay period as deposition and coagulation depleted the numbers of the smallest particles (Figure 2). About 95% of the particles at the beginning of the decay period had diameters of <10 nm. For the stovetop burners, the <10 nm particles were more numerous, by factors of 4 to nearly 30, than the >10 nm particles. Assuming uniform distribution throughout the test house, and ignoring losses due to air change and deposition on surfaces, the size-resolved emission rates per minute can be calculated. These estimates are expected to be somewhat conservative, since the source was in a separate room from the SMPS and particles were lost to processes such as coagulation and deposition while in transit to the MBR. The total number of <10 nm particles produced by the gas burners alone was in the range of 10^{12} to 10^{13} min^{-1}. For the nine experiments with the SMPS in the kitchen, the peak concentrations of particles of all sizes were 4−8 times the concentrations measured in the bedroom, with peak values exceeding 10^6 particles/cm^3. The stovetop burners consistently produced size distributions with geometric mean diameters considerably less than 10 nm (range 4−7 nm). The gas oven and broiler generally produced larger particles, with geometric means ranging up to 24 nm.

Results from the 36 experiments involving cooking food or boiling water on the gas stove are provided in Table S2, Supporting Information. Size distributions produced by bringing different amounts of water (350 and 700 mL) to a boil on the stovetop burner peaked at particle diameters from 5 to 7 nm. The emission rate from boiling different amounts of water was about 6×10^{12} min^{-1}. The use of cooking oil while stir-frying vegetables and frying eggs and bacon shifted the distribution toward larger particles, with peak concentrations occurring in the 16−20 nm range. Baking or broiling food in the gas oven consistently resulted in 2−3 times more >10 nm particles than <10 nm particles. The baking mode used gas at a rate of 5.1 (SD = 1.1) L/min, the broiling mode at a higher rate of 7.1 (SD = 0.3) L/min.

The potential exposure associated with cooking in the kitchen was studied in a series of experiments with the SMPS in the kitchen rather than the MBR. Three experiments boiling 350 and 700 mL of water in the kitchen resulted in peak concentrations ranging from 430 000 to 680 000 cm^{-3}. The same amounts of water boiled for the same amount of time resulted in concentrations ranging from 27 000 to 47 000 cm^{-3} in the MBR.

The geometric mean diameters tended to increase (from 5−6 to 16−20 nm) if cooking oil was used, whereas maximum concentrations and emission rates decreased (Table S2, Supporting Information). This may reflect the loss of detection efficiency that has been noted before for the water-based CPC when challenged by oil droplets (*27*).

Electric Stove. Results from the electric stove experiments are provided in Table S3, Supporting Information. Heating the stovetop coils alone or boiling water on them tended to produce about 2−5 times more <10 nm particles than >10 nm particles. Geometric mean diameters ranged from about 6 to 8 nm. Heating oil in a pan or cooking food on the stovetop coils resulted in a preponderance of >10 nm particles, with geometric mean diameters between 12 and 25 nm (Figure S2, Supporting Information). The electric oven and broiler (heated without food) produced many fewer particles of all sizes than the stovetop coils, with emission rates for <10 nm particles ranging between 4×10^{10} and 7×10^{10} min^{-1} and rates for >10 nm particles of 2×10^{11} min^{-1}.

Experiments with the stovetop coil set to its highest setting for 4 min were carried out on the right rear ($N = 4$) and left front ($N = 3$) burners. The right rear coil had never been used before, and the first experiment resulted in many more >10 nm particles than the next three. The left front coil had been used before, the last time about 3 months earlier, and the first experiment with it also showed more large particles than the next two experiments (Figure S3, Supporting Information). This trend was repeated with all four electric stovetop coils, suggesting that either the coating on the coils

TABLE 1. Summary of Results from 150 Tests of Three Kitchen Appliances[a]

mode	no. of tests	geometric mean diameter (nm)	peak concn (2−64 nm) ($\times 10^3$ cm^{-3})	emission rate ($\times 10^{12}$ min^{-1})
		Gas Stove: No Food Cooked		
burner (SMPS in Kitchen)	9	4.4–7.0	290–2200	N/A
burner (SMPS in MBR)	19	4.0–7.0	90–740	4.6–13
oven (bake/broil)	14	4.3–24	48–450	0.3–5.1
		Gas Stove: Food Cooked or Water Boiled		
burner (SMPS in kitchen)	1	8.7	1000	N/A
burner (SMPS in MBR)	11	5.5–20	24–190	0.4–7.0
oven (bake/broil)	5	4.6–18	22–140	0.4–1.1
		Electric Stove		
stovetop coil: no food cooked	31	3.2–22	7.1–350	0.6–11
stovetop coil: food cooked	31	6.1–31	9.0–310	0.14–14
oven (bake/broil): no food cooked	12	5.2–30	3.3–47	0.06–0.8
		Electric Toaster Oven		
oven in MBR: no food cooked	5	28–32	740–1500	3.1–6.4
oven in kitchen: no food cooked	7	16–18	230–340	4.1–6.0
oven in MBR: food cooked	6	22–49	31–210	1.8–3.7

[a] Note: Uncertainties associated with these values include the 12% uncertainty in number concentrations for an individual size category. However, since the total number is summed across 97 categories, the resultant uncertainty is substantially reduced. Tables S1−S3 in the Supporting Information provide means and associated standard deviations for individual tests.

or collected dust following periods of disuse were providing a transient contribution to concentrations of >10 nm UFPs.

Cooking 120 mL of rice with 240 mL of water in a saucepan on the small coil produced particles peaking at about 20 nm, with few <10 nm particles. Sauteeing peanut oil in a frying pan on the large front coil resulted in a size distribution peaking at about 35 nm, with fewer than 5% of the particles being <10 nm. Frying bacon and eggs with olive oil on that coil and toasting an English muffin in the broiler also resulted in few <10 nm particles.

Electric Toaster Oven. Results from the toaster oven experiments are provided in Table S4, Supporting Information. For the extreme conditions associated with the toaster oven in the MBR with the doors closed, concentrations of the >10 nm particles exceeded 1 million per cubic centimeter. These concentrations were about 4 times the levels reached in the MBR when the toaster oven was operated in the kitchen. Emission rates for >10 nm particles were in the range of 3×10^{12} to 6×10^{12} min^{-1}, about an order of magnitude greater than the rates for the smaller particles. The geometric mean diameter during the decay period ranged from 28 to 32 nm in the MBR but only from 16 to 18 nm when the toaster oven was in the kitchen (Figure S4, Supporting Information), probably due to extensive coagulation in the MBR at the very high concentrations reached during the production period, which led to depletion of the smaller particles.

Selected results from the tests of all three appliances are provided in Table 1. More detailed results are given in Tables S1−S4 of the Supporting Information.

Air Change Rates and Indoor/Outdoor Ratios. Air change rates were measured for each of the approximately 150 experiments taking place over more than one year. Because the test house was uninhabited and had closed windows during most of the tests, the air change rates were low and showed little variation (mean 0.23 h^{-1}, SD = 0.13 h^{-1}, range 0.097−0.57 h^{-1}).

The indoor/outdoor ratios were <0.05 for all <10 nm particles, rising monotonically to 0.20 for particles near 60 nm in diameter.

Coagulation. Coagulation rates are very large and rapidly changing during the first 20 min of the decay period. In a gas burner experiment, the coagulation rates varied from about +13 to −7 h^{-1} for different size categories during the first 2.5 min of the decay period. (A negative rate indicates a gain in number concentration for the associated particle size.) These rates are far higher than the typical air change rates for this test house of 0.1−0.3 h^{-1} and the theoretical deposition rates of <0.5 h^{-1} for all but the smallest particles. A comparison of the three mechanisms (coagulation, deposition, and air change rates) as they affect number concentration changes between scans is provided in Figure 3; this general dominance of coagulation was repeated in most experiments. A preliminary estimate of the total number concentration at which coagulation is no longer dominant compared to air exchange and deposition was <30 000 cm^{-3}; at that concentration, the loss rate due to coagulation in one experiment was still approximately double the rates due to either air change or deposition. This value is less than the 100 000 cm^{-3} estimate found in many textbooks, but since we are considering the

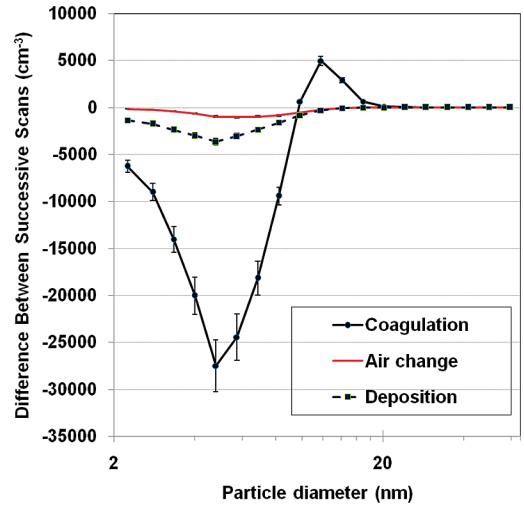

FIGURE 3. Particle losses/gains between two successive scans due to coagulation are compared to losses due to air change and deposition. The first scan was that with the highest total number concentration following shutoff of the source. Each particle size category is the sum of five contiguous size categories. Error bars are calculated using estimated uncertainties for the air change and coagulation rates and a nominal uncertainty of 10% for the theoretical estimates of deposition rates.

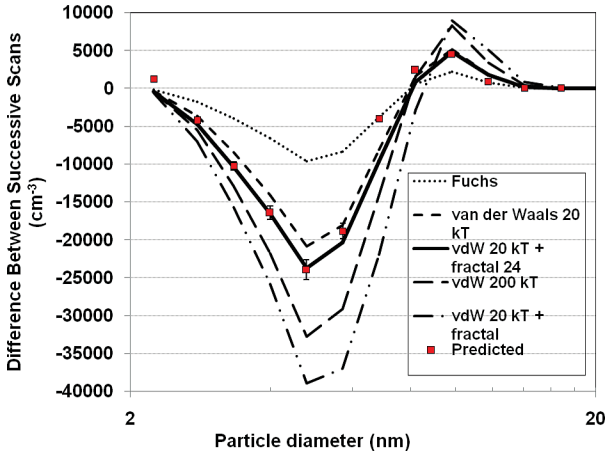

FIGURE 4. Comparison of five different coagulation models with predicted values based on observed number changes corrected for losses due to air change and deposition occurring in two successive scans. The best fitting model included a van der Waals/viscosity correction using a Hamaker constant of 20 *kT* multiplied by a correction due to assuming a fractal dimension of 1.7 for >24 nm particles. The first scan was the one with the highest total number concentration following shutoff of the source (gas burner 18 min experiment on May 1, 2007). Error bars take into account uncertainties associated with the number concentration estimates and the air change and deposition rates used in estimating the predicted coagulation rates.

<10 nm particles with their much higher Brownian motion, it seems reasonable.

The concentration losses due to the measured air change rates and estimated deposition rates (*25*) were subtracted from the observed concentration differences between scans. This remainder was called the "predicted" coagulation result. It was then compared to the calculated coagulation values using each of the six models in turn. The best fitting model was the one with the minimum sum of the absolute difference between the calculated and predicted values. An example of the results of applying several models to one experiment is given in Figure 4. In this figure, one model is clearly superior to the others in matching the predicted values. Additional examples of model fits for a gas stovetop burner and an electric stovetop coil are provided in Figures S5 and S6, Supporting Information. Note that in Figure S5, Supporting Information, only a small increase occurred for some size categories. Whether there is an increase depends on the shape of the size distribution.

For the particles produced by the gas stovetop burners and the electric stovetop coils, coagulation is the dominant process affecting their concentrations in the early part of the decay period. Coagulation rates for any given size category are dependent on the number concentrations of all other particles. The rates for a given particle size, unlike deposition rates, are not constant over time but vary according to the concentration changes in the other size categories.

The models described above were fit to the observed number concentration differences in successive scans (Table S5, Supporting Information). The model fitting the largest number of experiments was the van der Waals/viscosity model employing a Hamaker constant of 200 *kT* without a fractal correction. This was the only model providing the best fit to all eight of the electric toaster oven experiments amenable to model fitting. For the electric stovetop coils, the best fitting models were usually those with a fractal component (19 cases) rather than those without (6 cases). Results are mixed for the gas stovetop burners, with about as many cases showing a fractal character as not. The gas stove oven produced only three results in which coagulation models could provide reasonable fits, and the electric stove oven produced no cases with a good fit, probably due to insufficient numbers of particles to produce strong coagulation rates. Despite the fair amount of success in fitting the coagulation models to observations, there is a need for research on the composition and shape of the particles produced by these appliances and the associated Hamaker constants. Measured deposition rates are also needed to support or modify the theoretical estimates.

Emission Rates. How does the treatment of coagulation affect calculation of emission rates? Typically, the emission rate is calculated by assuming constant emission rates along with constant air change rates and deposition rates. These assumptions allow an analytical solution to the mass balance equation (*9*).

With coagulation, however, even if the source emission rate is constant over time for each size category, there is no longer a simple relationship with the number or mass concentration as a function of time. The number concentration for some size categories may increase for a time and then decrease *even while the source is still producing particles in that size category*. The reason is that the slower buildup of larger particles, which are more efficient at scavenging the smaller particles, ultimately results in loss rates for these smaller size categories greater than the gain due to generation by the source. This process was seen most clearly in the results from the three 2 h gas burner experiments. Many of the smallest particle sizes (<10 nm) reached their maximum concentrations within the first 15 min and then declined steadily for the next 105 min despite the burner remaining on. For the >10 nm particles, the time to reach the maximum value increased with particle size. Only particles larger than 30 nm in diameter were still increasing their concentration at the end of the 2 h period.

This behavior makes it difficult to estimate emission rates for the smaller particles. Rates will appear to be dependent on the time spent cooking, with high rates for short cooking periods and lower rates for longer periods. The time-averaged rates we report are therefore underestimates of the true rates; on the other hand, they provide more realistic estimates of resulting concentrations since they include the effect of coagulation.

Another effect leading to underestimation of the emission rates is the assumption of perfect instantaneous mixing. The SF_6 measurements showed that a single 10 min injection at one point in the house required about 40 min to reach a well-mixed condition. Since most of our cooking times were shorter than 40 min, and most of our measurements were in the nonsource room, this will lead to underestimates of the emission rates. The amount of the underestimate due to this effect is difficult to calculate; however, measurements made using a second CPC (described in the Supporting Information) indicated that concentrations measured in the master bedroom while the source was on were typically 20% lower than those in the other nonsource rooms in the house.

Previous studies on emission rates of ultrafine particles from cooking are limited. Emission rates of 0.35×10^{11} to 7.34×10^{11} min^{-1} were reported for multiple types of cooking in 15 homes in Brisbane (*11*), for >15 nm particles. A mean rate of 3.3×10^{12} min^{-1} was reported for 24 cooking events on a gas stove in one house in Virginia (*9*), for >10 nm particles. The rates reported in the present study varied from 10^{11} to 10^{13} min^{-1}.

Mean number concentrations ranged from 16 000 to 179 000 cm^{-3} in Brisbane (*11*) and about 100 000 cm^{-3} in Virginia (*9*), compared to the range in the present study from 30 000 to 600 000 cm^{-3}. For the worst-case scenarios in the present study, involving measurements in the same room as the gas stove or the electric toaster oven, the concentrations ranged upward to 1 500 000 cm^{-3}, about a factor of 10 higher

than previous reported maxima, with most of this increase due to the <10 nm particles.

Exposure Implications. Typical peak concentrations following as little as 4 min of boiling a small amount of water reached 100 000 cm^{-3}, compared to the typical background of about 1000 cm^{-3}. Although coagulation reduces this number much faster than air change and deposition, concentrations still remain elevated for about 2 h. Although concentrations during cooking were several times higher in the kitchen than in the other rooms, the room-to-room gradient does not last long due to inter-room transport. Therefore, we expect the long-term exposure of the cook to be not greatly increased compared to that of other inhabitants. However, all inhabitants will be exposed to greatly increased UFP concentrations for a period of time following use of the stovetop burners/coils.

Exposures can be substantially reduced by using range hoods ventilated outside. However, the design of the hood and the flow rate of the fan should be properly chosen to provide high efficiency. Some studies have indicated that poor design and low efficiencies are common. In the case of the <10 nm particles, it is possible that their increased Brownian motion will lower the efficiency of range ventilation.

A multiyear study in an inhabited house concluded that 80% of total exposure to particles between 10 and 50 nm in diameter, and 60% of total exposure to particles between 50 and 100 nm in diameter, was due to indoor sources (*28*). The present study suggests that this trend is also valid for particles less than 10 nm in diameter. These <10 nm particles have difficulty in penetrating homes and deposit faster than larger ultrafine particles, as shown by the indoor/outdoor ratios of <0.05. They are also produced in large quantities by common indoor sources such as gas and electric stoves. Therefore, a large fraction of exposure to these <10 nm particles also is likely to be due to indoor sources.

In summary, gas and electric stovetop burners/coils emit large numbers of ultrafine particles smaller than 10 nm in diameter. Emission rates for <10 nm particles are in the range of 10^{12} particles/min, resulting in concentrations of about 10^5 particles cm^{-3} in a 340 m^3 house following cooking. Coagulation rates are very high for these particles at these concentrations. The composition, morphology, and potential health effects of these particles are not established.

Acknowledgments

Steven Emmerich and Steven Nabinger operated the NIST test house air change and pressure−temperature−humidity devices. Brian Polidoro of NIST prepared the program to calculate the Brownian coagulation coefficients. We thank William W. Nazaroff of the University of California, Berkeley, for supplying the spreadsheet used to calculate deposition rates. We are grateful to Mark Z. Jacobson of Stanford University for sharing the computer program used to determine the effect of van der Waals and viscocity forces and fractal shapes on the Brownian coagulation coefficient. We also thank four anonymous reviewers for their valuable comments. The full description of the procedures used in this paper requires the identification of certain commercial products and their suppliers. The inclusion of such information should in no way be construed as indicating that such products or suppliers are endorsed by NIST or are recommended by NIST or that they are necessarily the best materials, instruments, software, or suppliers for the purposes described.

Supporting Information Available

Further details regarding the measurement methods for particles and tracer gas, derivation of the algorithm for calculating the coagulation kernel with the Fuchs correction for the 97 size categories available on the SMPS, detailed tables breaking out the concentrations and emission rates for <10 and >10 nm particles, and six figures including a floor plan of the research house, size distributions created by cooking on the electric stove and electric toaster oven, and model fits for coagulation calculations. This information is available free of charge via the Internet at http://pubs.acs.org.

Literature Cited

(1) Oberdörster, G.; Oberdörster, E.; Oberdörster, J. Nanotoxicology: An emerging discipline evolving from studies of Ultrafine particles. *Environ Health Perspect.* **2005**, *113*, 823–839.
(2) Bräuner, E. V.; Forchhammer, L.; Møller, P.; Simonsen, J.; Glasius, M.; Wåhlin, P.; Raaschou-Nielsen, O.; Loft, S. Exposure to ultrafine particles from ambient air and oxidative stress-induced DNA damage. *Environ. Health Perspect.* **2007**, *115*, 1177–1182.
(3) Bräuner, E. V.; Forchhammer, L.; Møller, P.; Barregard, L.; Gunnarsen, L.; Afshari, A.; Wåhlin, P.; Glasius, M.; Dragsted, L. O.; Basu, S.; Raaschou-Nielsen, O.; Loft, S. Indoor particles affect vascular function in the aged: An air filtration-based intervention study. *Am. J. Resp. Crit. Care Med.* **2007**, *177*, 419–25.
(4) Stölzel, M.; Breitner, S.; Cyrys, J.; Pitz, M.; Wölke, G.; Kreyling, W.; Heinrich, J.; Wichmann, H.-E.; Peters, A. Daily mortality and particulate matter in different size classes in Erfurt, Germany. *J. Exposure Sci. Environ. Epidemiol.* **2007**, *17*, 458–467.
(5) Kleeman, M. J.; Schauer, J. J.; Cass, G. R. Size and composition distribution of fine particulate matter emitted from motor vehicles. *Environ. Sci. Technol.* **2000**, *34*, 1132–1142.
(6) Zhang, Q.; Stanier, C. O.; Canagaratna, M. R.; Jayne, J. T.; Worsnop, D. R.; Pandis, S. N.; Jimenez, J. L. Insights into the chemistry of new particle formation and growth events in Pittsburgh based on aerosol mass spectrometry. *Environ. Sci. Technol.* **2004**, *38*, 4797–4809.
(7) Dennekamp, M.; Howarth, S.; Dick, C. A.; Cherrie, J. H. W.; Donaldson, K.; Seaton, A. Ultrafine particles and nitrogen oxides generated by gas and electric cooking. *Occup. Environ. Med.* **2001**, *58*, 511–516.
(8) Long, C. M.; Suh, H. H.; Catalano, P.; Koutrakis, P. Using time- and size-resolved particulate data to quantify indoor penetration and deposition behavior. *Environ. Sci. Technol.* **2001**, *35*, 2089–2099.
(9) Wallace, L. A.; Emmerich, S. J.; Howard-Reed, C. Emission rates of ultrafine and fine particles due to cooking with a gas stove. *Environ. Sci. Technol.* **2004**, *38*, 2304–2311.
(10) Klepeis, N. E.; Apte, M. G.; Gundel, L. A.; Sextro, R. G.; Nazaroff, W. W. Determining size-specific emission factors for environmental tobacco smoke particles. *Aerosol Sci. Technol.* **2003**, *37*, 780–790.
(11) He, C.; Morawska, L.; Hitchins, J.; Gilbert, D. Contribution from indoor sources to particle number and mass concentrations in residential houses. *Atmos. Environ.* **2004**, *38*, 3405–3415.
(12) Wallace, L. A. Ultrafine particles from a vented gas clothes dryer. *Atmos. Environ.* **2005**, *39*, 5777–5786.
(13) Wallace, L. A. Indoor sources of ultrafine and accumulation mode particles: Number concentrations and size distributions. *Aerosol Sci. Technol.* **2006**, *40*, 348–360.
(14) Chen, D.; Pui, D. Y. H.; Hummes, D.; Fissan, H.; Quant, F. R.; Sem, G. J. Design and evaluation of a nanometer aerosol differential mobility analyzer (nano-DMA). *J. Aerosol Sci.* **1998**, *29*, 497–509.
(15) U.S. Census Bureau American Housing Survey, 2005.
(16) Mulholland, G.; Donnely, M.; Hagwood, C.; Kukuck, S.; Hackley, V. A. Measurement of 100nm and 60nm particle standards by differential mobility analysis. *J. Res. Natl. Inst. Stand. Technol.* **2006**, *111*, 257–312.
(17) TSI. *Model 3786 Ultrafine Water-Based Condensation Particle Counter Operation and Service Manual*; P/N 1930072, revision B; Shoreview, MN, April 2005.
(18) Mordas, G.; Manninen, H. E.; Petäjä, T.; Aalto, P. P.; Hämeri, K.; Kulmala, M. On operation of the ultra-fine water-based CPC TSI 3786 and comparison with other TSI models (TSI 3776, TSI 3772, TSI 3025, TSI 3010, TSI3007). *Aerosol Sci. Technol.* **2008**, *42*, 152–158.
(19) TSI. *Scanning Mobility Particle Sizer™ (SMPS™) Spectrometer Diffusion Loss Correction*; Application Note SMPS-001; Shoreview, MN, 2006.
(20) American Society for Testing and Materials. ASTM E741-00(2006) Standard Test Method for Determining Air Change in a Single

Zone by Means of a Tracer Gas Dilution. http://www.astm.org/cgi-bin/SoftCart.exe/DATABASE.CART/REDLINE_PAGES/E741.htm?E+mystore (accessed April 17, 2006).
(21) Seinfeld, J. H.; Pandis, S. N. *Atmospheric Chemistry and Physics*, 2nd ed.; Wiley: New York, 2006.
(22) Jacobson, M. Z.; Seinfeld, J. H. Evolution of nanoparticle size and mixing state near the point of emission. *Atmos. Environ.* **2004**, *38*, 1839–1850.
(23) Visser, J. On Hamaker constants: A comparison between Hamaker constants and Lifshitz−van der Waals constants. *Adv. Colloid Interface Sci.* **1972**, *3*, 331–363.
(24) Jacobson, M. Z. *Fundamentals of Atmospheric Modeling*, 2nd ed.; Cambridge University Press: Cambridge, England, 2005.
(25) Dobbins, R. A. Hydrocarbon nanoparticles formed in flames and diesel engines. *Aerosol Sci. Technol.* **2007**, *41*, 485–496.
(26) Lai, A. C. K.; Nazaroff, W. W. Modeling indoor particle deposition from turbulent flow onto smooth surfaces. *J Aerosol Sci.* **2000**, *31*, 463–476.
(27) TSI. *Measuring Nanoparticle Size Distributions in Real-Time: Key Factors for Accuracy*; Application Note SMPS-003; Shoreview, MN.
(28) Wallace, L. A.; Howard-Reed, C. Continuous monitoring of ultrafine, fine, and coarse particles in a residence for 18 months in 1999−2000. *J. Air Waste Manage. Assoc.* **2002**, *52*, 828–844.

ES801402V